Journal of Science and Technology in Civil Engineering, NUCE 2021. 15 (3): 157–170

ACOUSTIC BEHAVIOR PREDICTION OF MONODISPERSE FOAMS USING POLYNOMIAL SURROGATES

Van-Hai Trinh[a,*]

[a]*Faculty of Vehicle and Energy Engineering, Le Quy Don Technical University, 236 Hoang Quoc Viet street, Bac Tu Liem district, Hanoi, Vietnam*

Article history:
Received 26/05/2021, Revised 15/07/2021, Accepted 16/07/2021

Abstract

Acoustic properties of foams, such as macroscopic transports and sound absorption, are significantly influenced by their local morphology. The present paper develops a polynomial chaos expansion (PCE)-based surrogate model for characterizing the microstructure-properties relationships of acoustic monodisperse foams. First, the acoustic properties of the considered structures are estimated numerically by homogenization techniques using an idealized periodic unit cell and the Johnson-Champoux-Allard-Pride-Lafarge (JCAPL) model. The reference maps of transport parameters are then used to construct the PCE–based surrogates in the design space involving a set of foamy microstructural parameters such as membrane content, cell size, and porosity. Finally, after a validation phase and assessing convergence characteristics, the generated surrogates are employed to design some foam-based absorbers to illustrate the accuracy and computational efficiency of the proposed method.

Keywords: membrane foam; transport property; sound absorption; multiscale simulation; polynomial surrogate.

https://doi.org/10.31814/stce.nuce2021-15(3)-13

1. Introduction

In noise engineering, one of the most common problems raised in recent years is finding materials or structures with the desired sound absorption performance [1–3]. Compared with other traditional solutions (i.e., fibrous or granular), cellular materials or solid foams have been developed and widely applied for various fields due to their acoustic properties [4–6] and other relevant advantages such as their lightweight and high specific surface area [7]. This sound-absorbing material is a highly porosity cellular structure that can absorber partially the energy of the sound wave propagating inside. By controlling the foamy morphology features, the desirable sound absorption coefficient of a given foam-based absorber can be achieved at the considered frequency bands (e.g., low or high frequency targets [8]).

Methodologically, to characterize sound absorbing materials, three main approaches are widely used, namely the phenomenological, semi-phenomenological, and empirical ones. These methods are supported by analytical, numerical, and experimental developments and techniques. In the equivalent-fluid method [2], a porous medium with a rigid frame is represented by an effective density and an effective bulk modulus, this serves a powerful framework for modeling and characterizing the functional properties of studied materials. Numerically, these macro-scale complex parameters can be

*Corresponding author. *E-mail address:* hai.tv@lqdtu.edu.vn (Trinh, V.-H.)

defined using two alternative ways based on finite element method (FEM): direct numerical simulations [9] and multiscale homogenization (direct [10, 11] and hybrid [4, 12, 13] schemes). In the direct multiscale calculation, the effective properties are directly formed from the calculated dynamic viscous and thermal permeability functions. The hybrid multiscale calculation allows computing the characteristic lengths and transport factors. From these macroscopic transports, the effective properties are also calculated through the corresponding semi-phenomenological models (e.g., JCAPL model). Experimentally, standing impedance tube measurements can be used to undertake the above parameter estimations [14–16].

To address the computational burden of time-consuming system simulations for characterizing materials, a meta-model or surrogate model can be a potential candidate. Modeling seems to take computing cost depending the level of structure complex, while surrogating is technique we can formulate the system response or map based on a scare or less computed data. Using the surrogate model, we can generate analytically any points in the input space for investigating and searching the global or target criteria. Surrogate modeling techniques (e.g., neural network [17], multivariate polynomials [18]) are therefore often used for establishing the link between the input variables and the functional responses of acoustic systems (e.g., absorber, anechoic [19]). The aim of this paper is to generate a PCE-based surrogate model for predicting the acoustic absorption of membrane foams. The surrogate is reconstructed based on the reference map that is deduced from the multiscale computations.

The paper is organized as follows. Section 2 provides briefly multi-scale modeling of acoustic foam materials with hybrid numerical homogenization via reconstructed Kelvin unit cell. In Section 3, the reference map of transport parameters is used to construct the surrogates. Section 4 illustrates the computational efficiency and predictability of the generated surrogates for designing some foam-based absorbers after a verification work. Conclusions are finally provided in Section 5.

2. Multi-scale modeling of foam structure

2.1. Foamy morphology and periodic unit cell

Foamy structure is made of membranes or films, ligaments or Plateau's borders (junction of three membranes) and vertices or nodes (junction of four ligaments), see Fig. 1(a). Whereas closed membranes are necessary to ensure the mechanical stability of liquid foam [20, 21], membranes can be open or totally absent in solid foams, allowing for the foam cells (pores) to be connected through windows.

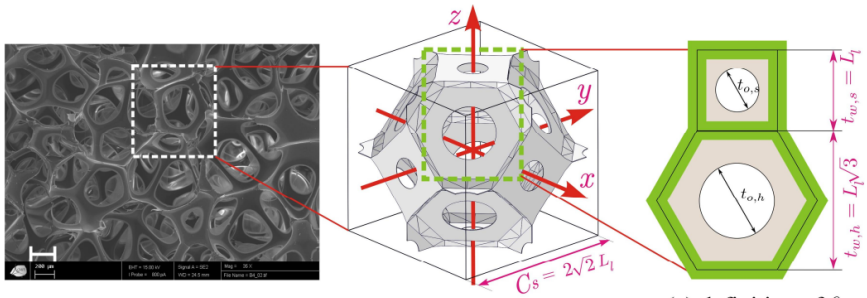

(a) SEM image of real foam (b) Kelvin unit cell (c) definition of δ_c

Figure 1. Modeling local microstructure of monodisperse foams with membranes

A periodic unit cell (PUC) having a size C_s (Fig. 1(b)) is used to represent the structure of monodisperse foam materials. The cell is based on the Kelvin pattern and counted 14 faces (8 hexagons and 6 squares). As we are mostly interested in the effect of the closure ratio of windows, the unit cell is made of idealized ligament having a length $L_l = C_s/(2\sqrt{2})$ and an equilateral triangular cross section with edge side r [21],

$$r \approx C_s \sqrt{\frac{1-\phi}{3\sqrt{3}/\sqrt{2} - \left(10 - 3\sqrt{6}\right)\sqrt{(1-\phi)\ \sqrt{2}/3\sqrt{3}}}} \tag{1}$$

For each window, the closure ratio of membrane is defined as:

$$\delta_c = 1 - \sqrt{A_{ap}/A_{po}} \tag{2}$$

where A_{ap} is the aperture area (the area of the aperture circles with diameter t_{os} and t_{oh}), and A_{po} is the window area (the area of the corresponding polygonal face with edge size of t_{ws} and t_{wh}) see Fig. 1(c).

Using the PUC configuration Ω (within fluid phase Ω_f and solid-fluid interface $\partial\Omega_f$), the purely geometrical parameter the thermal characteristic length Λ' also named as hydraulic radius can be estimated by

$$\Lambda' = 2\iiint_{\Omega_f} dV \Big/ \iiint_{\partial\Omega_f} dS \tag{3}$$

2.2. Numerical calculations of transport parameters

This section presents the first-principles calculations of six transport properties (e.g., the thermal and viscous permeabilities, the thermal and viscous characteristic lengths, and static and high frequency tortuosities).

a. Stokes equation with no-slip boundaries

At the low frequency limit (when $\omega \to 0$), in the pore domain of porous media, viscous effects dominate, and a steady-state flow is created. This flow of an incompressible Newtonian fluid at very low Reynolds numbers is governed by the usual Stokes equations as [22]

$$\begin{aligned} \eta\Delta\mathbf{v} - \nabla \mathrm{p} = -G \text{ with} \quad & \nabla\cdot\mathbf{v} = 0 \text{ in } \Omega_f \\ \mathbf{v} = 0 \quad & \text{on } \partial\Omega_f \end{aligned} \tag{4}$$

where $\mathbf{v}$, p, and η are respectively the velocity, pressure, and viscosity of the fluid. In general, $G = \nabla p^m$ is a macroscopic pressure gradient acting as a source term. Symbols Δ and ∇ are respectively the Laplacian and nabla differential operators, while "$\cdot$" denotes the classical inner product in $\mathbb{R}^3$. The local static viscous permeability can be obtained from the local velocity field as,

$$v = -1/\eta\, k_0^* G \tag{5}$$

Then, the components of the static viscous permeability tensor $\mathbf{k}_0$ and the static viscous tortuosity tensor $\boldsymbol{\alpha}_0$ are calculated as [23],

$$k_{0ij} = \phi\left\langle k_{0ij}^*\right\rangle; \quad \alpha_{0ij} = \frac{\left\langle k_{0pi}^* k_{0pj}^*\right\rangle}{\left\langle k_{0ii}^*\right\rangle\left\langle k_{0jj}^*\right\rangle}, \quad 1 \le i \le j \le 3, \tag{6}$$

where p is the Einstein summation notation, and the symbol $\langle \bullet \rangle$ indicates a fluid-phase average formulated by $\langle \bullet \rangle = 1/|\Omega_f| \iiint_{\Omega_f} \bullet dV$. It can be noted that referring to a symmetry feature of the considered geometry, the second-order transport tensors $\mathbf{k}_0$ and $\boldsymbol{\alpha}_0$ are isotropic (i.e., $k_{0ij} = k_0\delta_{ij}$ and $\alpha_{0ij} = \alpha_0\delta_{ij}$ where δ_{ij} is the Kronecker symbol). It means that the definition of these static transport parameters can be as a scalar instead of their full form of a second-order tensor.

b. Conduction problem with insulation boundaries

In high-frequency regime, when ω large enough (i.e., $\omega \to \infty$), inertial forces dominate over viscous ones and the saturating fluid tends to behave as a nearly ideal one without viscosity except in the vicinity of the boundary layer. In this case, the inertial flow of the perfect incompressible fluid formally behaves according to the electric conduction phenomenon [24]. Consequently, the quantities of interest in the inertial flow problem be obtained by solving the following set of potential equations:

$$\begin{aligned} &\nabla \cdot \mathbf{E} = 0 \quad \text{with} \quad \mathbf{E} = -\nabla\varphi + \mathbf{e} && \text{in } \Omega_f \\ &\mathbf{E} \cdot \mathbf{n} = 0 && \text{on } \partial\Omega_f \end{aligned} \tag{7}$$

where $\mathbf{e}$ is a given macroscopic electric field, $\mathbf{E}$ is the local solution of the boundary problem having $-\nabla\varphi$ as a fluctuating part, and $\mathbf{n}$ is the unit normal to the boundary of the pore region $\partial\Omega_f$. Herein, assuming that porous material composes of a non-conductive solid matrix and a conductive fluid.

The components of the viscous characteristic length tensor $\boldsymbol{\Lambda}$ and the through thickness high-frequency tortuosity tensor $\boldsymbol{\alpha}_\infty$ can be calculated as [25],

$$\Lambda_{ij} = 2\frac{\iiint_{\Omega_f} \mathbf{E}_{pi}\mathbf{E}_{pj}dV}{\iint_{\partial\Omega_f} \mathbf{E}_{pi}\mathbf{E}_{pj}dS}; \quad \alpha_{\infty ij} = \frac{\langle \mathbf{E}_{pi}\mathbf{E}_{pj} \rangle}{\langle \mathbf{E}_{ii} \rangle \langle \mathbf{E}_{jj} \rangle} \tag{8}$$

c. Heat equation with isothermal boundaries

At the low frequency limit (i.e., in the static case), heat diffusion in porous media is governed by the Poisson equation [26],

$$\begin{aligned} \nabla^2\tau &= -1 && \text{in } \Omega_f \\ \tau &= 0 && \text{on } \partial\Omega_f \end{aligned} \tag{9}$$

From the obtained field τ over the whole representative cell, the static thermal permeability is defined as the average value of the field solution, while the static thermal tortuosity is estimated similarly to the path for two above tortuosity functions. These factors are estimated as [24]

$$k_0' = \langle \tau \rangle; \quad \alpha_0' = \langle \tau^2 \rangle / \langle \tau \rangle^2 \tag{10}$$

The full set of above estimated transport parameters is used to describe the sound absorbing layer with effective properties through the semi-phenomenological model in the next section.

2.3. Estimation of sound absorption

Following the equivalent-fluid theory, the effective density and the effective bulk modulus are defined in the semi-phenomenological model (i.e., JCALP model) as following equations [25, 27, 28]

$$\tilde{\rho}(\omega) = \frac{\rho_0\alpha_\infty}{\phi}\left[1 + \frac{1}{j\varpi'}\left(1 - P + P\sqrt{1 + \frac{M}{2P^2}j\varpi}\right)\right] \tag{11}$$

$$\tilde{K}(\omega) = \frac{\gamma P_0}{\phi}\left\{\gamma - (\gamma-1)\left[1 + \frac{1}{j\varpi'}\left(1 - P' + P'\sqrt{1 + \frac{M'}{2P'^2}j\varpi'}\right)\right]^{-1}\right\}^{-1} \tag{12}$$

with

$$\varpi = \frac{\omega}{\nu}\frac{k_0\alpha_\infty}{\phi};\ \ \varpi' = \frac{\omega}{\nu'}\frac{k'_0}{\phi} \tag{13}$$

$$M = \frac{8\alpha_\infty}{k_0\Lambda^2\phi};\ \ P = \frac{M}{4(\alpha_0/\alpha_\infty - 1)};\ \ M' = \frac{8k'_0}{\Lambda'^2\phi};\ \ P' = \frac{M}{4(\alpha'_0 - 1)} \tag{14}$$

where ρ_0 denotes the density of the saturating fluid (i.e., air), $\gamma = C_p/C_v$ is the ratio of the pressure volume-specific heat C_p and the constant pressure-specific heat C_v, P_0 is the atmospheric pressure, $\omega = 2\pi f$ is the angular frequency. Four non-dimensional shape factors M, M', P, and P' depend on material transport parameters including the open porosity ϕ, the thermal and viscous characteristic lengths (Λ', Λ), the static viscous and thermal permeabilities $\left(k_0, k'_0\right)$, the high frequency tortuosity α_∞, and the static tortuosities $\left(\alpha_0, \alpha'_0\right)$.

Then, the wavenumber $\tilde{k}(\omega)$ and the characteristic impedance $\tilde{Z}_c(\omega)$ of the homogeneous acoustic layer can be calculated as

$$\tilde{k}(\omega) = \omega\sqrt{\frac{\tilde{\rho}(\omega)}{\tilde{K}(\omega)}};\ \ \tilde{Z}_c(\omega) = \sqrt{\tilde{\rho}(\omega)\tilde{K}(\omega)} \tag{15}$$

Under normal incidence acoustic plane wave, the sound absorption coefficient of an sound absorber backed by a rigid wall (i.e., without airgap) is defined as

$$A_\alpha(\omega) = 1 - \left|\frac{j\tilde{Z}_c(\omega)\cot[\tilde{k}(\omega)L] - Z_0}{j\tilde{Z}_c(\omega)\cot[\tilde{k}(\omega)L] + Z_0}\right|^2 \tag{16}$$

where Z_0 is the characteristic impedance of ambient air, and L is the layer thickness.

3. Polynomial chaos expansion-based surrogate

Using the reference maps of several above-estimated transport parameters, the general polynomial expansion techniques present as follows are used to construct the surrogate model describing structure-transport relationships of foams.

3.1. Polynomial chaos expansion

Since the reference map $\mathbf{m} \mapsto \mathbf{q}(\mathbf{m})$, with $\mathbf{m}$ belongs to some admissible closed set $\mathbf{S}_m = \times_{i=1}^{d}[a_i, b_i]$ in $\mathbb{R}^d$, typically introduces some smoothness due to its multiscale nature, polynomial approximation techniques are natural candidates for the construction of the surrogate map $\hat{\mathbf{q}}$ and are considered thereafter. Upon introducing the normalized vector-valued parameter $\boldsymbol{\xi} = \{\xi_i\}_i^d$ with $\xi \in [-1, 1]$ such that:

$$\xi_i := 2m_i/(b_i - a_i) + (a_i + b_i)/(a_i - b_i) \tag{17}$$

The surrogate model $\hat{\mathbf{q}}$ is then sought for as a polynomial map in $\boldsymbol{\xi}$:

$$\hat{\mathbf{q}}(\boldsymbol{\xi}) = \sum_{\alpha,|\alpha|=0}^{+\infty} \boldsymbol{\psi}_\alpha \mathbf{P}_\alpha(\boldsymbol{\xi}) \tag{18}$$

where $\boldsymbol{\alpha}$ is a multi-index in $\mathbb{N}^d$ with $|\boldsymbol{\alpha}| = \sum_{i=1}^{d} \alpha_i$, and $\mathbf{P}_{\alpha}(\boldsymbol{\xi}) = \prod_{i=1}^{d} P_{\alpha_i}(\xi_i)$ is a the multidimensional Legendre polynomial with $P_{\alpha_i}(\xi_i)$ is the univariate Legendre polynomial of order α_i [29], given as with $\alpha_i \geq 1$:

$$P_{\alpha_i+1}(\xi) = \frac{2\alpha_i + 1}{\alpha_i + 1}\xi P_{\alpha_i}(\xi) - \frac{\alpha_i}{\alpha_i + 1}\xi P_{\alpha_i - 1}(\xi) \tag{19}$$

in which two first polynomials as $P_0(\xi) = 1$ and $P_1(\xi) = \xi$.

From the orthogonality of these polynomials, namely,

$$\mathbb{E}\left\{\mathbf{P}_{\alpha}\mathbf{P}_{\beta}\right\} := \frac{1}{2^d}\int_{[-1,1]^d} \mathbf{P}_{\alpha}(\mathbf{x})\mathbf{P}_{\beta}(\mathbf{x})d\mathbf{x} = \prod_{i=1}^{d} \frac{\delta_{\alpha_i\beta_i}}{2\alpha_i + 1} \tag{20}$$

where δ_{ij} is Kronecker delta, it follows that

$$\boldsymbol{\psi}_{\alpha} = \left(\prod_{i=1}^{d}(2\alpha_i + 1)\right)\mathbb{E}\left\{\hat{\mathbf{q}}\mathbf{P}_{\alpha}\right\} \tag{21}$$

Let $\left\{\gamma_i, \hat{\boldsymbol{\xi}}_i\right\}_{i=1}^{n_Q}$ be the n_Q weights and integration nodes according to the Gauss-Legendre quadrature rule. The polynomial coefficients, for polynomial chaos expansion is truncated at order p, are thus approximated as

$$\boldsymbol{\psi}_{\alpha} = \frac{1}{2^d}\sum_{i=1}^{n_Q} \gamma_i \mathbf{q}\left(\hat{\boldsymbol{\xi}}_i\right) P_{\alpha}\left(\hat{\boldsymbol{\xi}}_i\right), \quad \forall \boldsymbol{\alpha} \in A_p \tag{22}$$

where $A_p = \left\{\boldsymbol{\alpha} \in \mathbb{N}^d : |\alpha| \leq p\right\}$, and $N = \text{card}\left(A_p\right) = (d + p)!(d!p!)$.

3.2. Reference sampling and convergence assessing

A periodic unit cell represented for cellular membrane foams is employed for a simple unit cell of the hybrid method. This unit cell is first reconstructed for cellular structure at porosity of ϕ having a given cell size of $C_s = 1$ mm and the closure membrane rate of δ_c (see Fig. 1). The membrane closed rate is varied in a range of $\delta_c = \left[\delta_c^{\min}, \delta_c^{\max}\right] = [0.1 \quad 0.9]$, while for foams within high porosity, the second variable is selected in a range of $\phi = \left[\phi^{\min}, \phi^{\max}\right] = [0.90 \quad 0.99]$.

From the above support $\mathbf{S}_m\,(d = 2)$ or $\boldsymbol{\xi} = (\xi_1, \xi_2)$, the considered map is introduced as $\mathbf{S}_q := (q_1, q_2, \ldots, q_7) = \left(\bar{\Lambda}', \bar{\Lambda}, \bar{k}_0, \bar{k}_0', \alpha_{\infty}, \alpha_0, \alpha_0'\right)$. Noted that herein four non-dimensional transport properties are evaluated as

$$\bar{\Lambda}'(\bar{\Lambda}) = \bar{\Lambda}'(\bar{\Lambda})/C_s; \quad \bar{k}_0\left(\bar{k}_0'\right) = k_0\left(k_0'\right)/C_s^2 \tag{23}$$

The convergence analysis with respect to the total number n_Q of quadrature points and the order p of the approximated expansion is evaluated with the error functions $n_Q \mapsto \varepsilon_{N_0}(n_Q)$ and $p \mapsto \varepsilon_p(p)$ below [30],

$$\varepsilon_{n_Q}(n_Q) = \left\|\psi_{\alpha}(n_Q + 1) - \psi_a(n_Q)\right\|^2 / \left\|\psi_{\alpha}(n_Q)\right\|^2 \tag{24}$$

$$\varepsilon_p(p) = \sqrt{\mathbb{E}\left\{\left(\hat{\mathbf{q}}_p(\boldsymbol{\xi}) - \mathbf{q}(\boldsymbol{\xi})\right)^2\right\}/\mathbb{E}\left\{\mathbf{q}^2(\boldsymbol{\xi})\right\}} \tag{25}$$

Finally, let ϑ_p be the relative error and measured as,

$$\vartheta_p = \left|\mathbf{q}(m) - \hat{\mathbf{q}}_p(m)\right|/\hat{\mathbf{q}}_p(m) \tag{26}$$

where $\hat{\mathbf{q}}_p$ is estimated from the p -order surrogate model.

To sum up the above-described method, the flow chart of modeling foams using polynomial surrogates is drawn in Fig. 2.

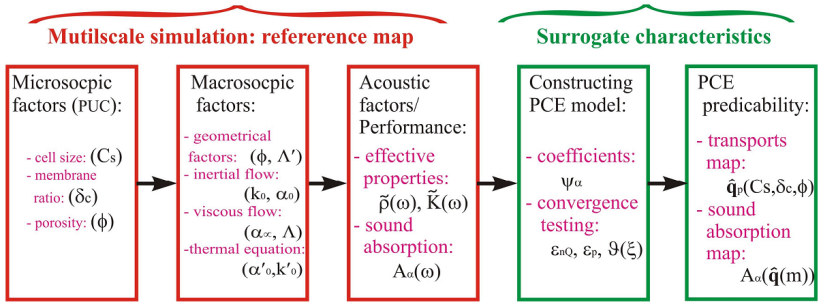

Figure 2. Flow chart of modeling foams using polynomial surrogates

4. Results and discussion

In this section, the characterization, the predictability, and the application of the PCE-based surrogate model are investigated and discussed.

4.1. Validation of FEM scheme and acoustic model

To validate the FEM scheme used for computing the reference map, we first employ it for a classical cubic lattice, i.e., face-centered cubic (FCC), see Fig. 3(a). This structure has a porosity of 0.24, sphere radius of 1 mm, and solder joints with a radius of 150 μm. First, the present computed transport properties are compared with the estimations in Ref. [10]. As listed in Table 1, a good agreement is obtained. Then, the sound absorbing coefficients are compared to demonstrate the consistent findings between the present hybrid numerical computation and the direct numerical one [10, 31]. The absorbers are based on the FCC packing (Fig. 3(a)) having two different thicknesses L = (50; 100) mm. The considered frequency ranges from 1 Hz to 10 kHz. In the direct approach, the SAC value is estimated from the effective factors taken from Table 3.4 and Table 3.5 in Ref. [31]. As shown in Figs. 3(c)–(d), the obtained curves of both absorbers reveal that the frameworks can predict consistently the acoustic behavior. The horizontal dashed line is the high-frequency sound absorption limit of 0.56 for the FCC pattern at a porosity ϕ = 0.26 [32]. The observations presented above strongly validate the proposed technique.

Table 1. Computed transport properties of the FCC structure

Reference	Λ' (mm)	Λ (mm)	k_0 ($\times 10^{-10}$ m^2)	k'_0 ($\times 10^{-10}$ m^2)	α_∞ (-)	α_0 (-)	α'_0 (-)
[10]	0.247	0.159	6.70	27.0	1.65	2.49	1.85
Present	0.247	0.157	6.76	26.3	1.66	2.65	1.89

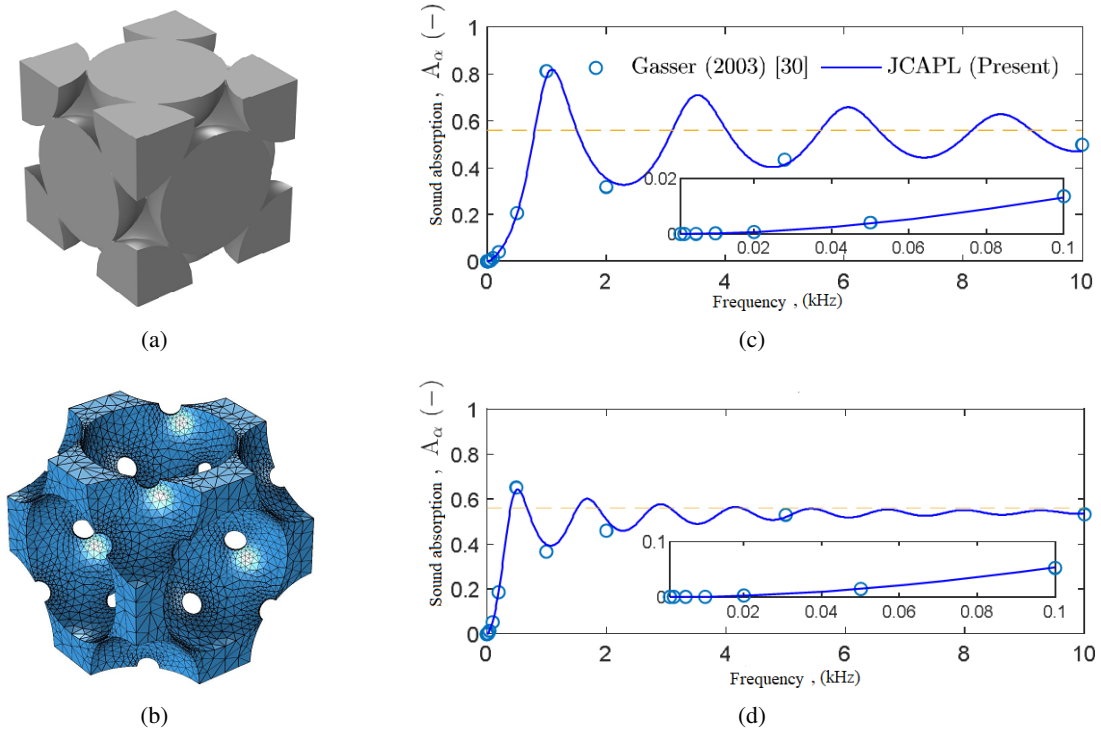

Figure 3. Solid domain (a) and mesh model of fluid phase (b) of PUC based on the FCC lattice. The sound absorption for the thickness of 50 mm (c) and 100 mm (d)

4.2. Assessment of the surrogate characteristics

The first convergence characteristic is investigated on the values of the polynomial coefficients. Fig. 4 presents several maps $n_Q \mapsto \varepsilon_{n_Q}(n_Q)$ for a set of four transports $\overline{\Lambda'}, \overline{k_0}, \overline{k_0'}$, and α_∞ as shown in sub-figure (a) to (d), respectively. The results are from left to right corresponding an increase in p, and the dash lines denote the tolerance value (i.e. $\varepsilon_Q = 10^{-2}$) except for the case of the purely geometrical factor, the thermal characteristic length with $\varepsilon_Q = 10^{-4}$. The curves state that with a given truncated order of polynomial expansion, we can select the optimal values of n_Q that provide the constraint tolerance error (see, solid markers). Noticed that for three remaining factors (i.e., $\bar{\Lambda}, \alpha_0$, and α_0'), similar observations can be made.

Next, within a high value of $n_Q = 20$, the L-norm error $\varepsilon_q(p)$ is measured for all seven macroscopic transport parameters as shown in Fig. 5. The results indicate clearly that the polynomial order of $p > 9$, the surrogate model can produce a least squared error, $\varepsilon < 10^{-2}$. In the considered range of p, it can be seen that the performance of the meta-model seems not to be improved by continuously increasing of order p except in the thermal characteristic length (see lines with square marker).

For sake of visibility, Fig. 6 depicts the distance mapping between the reference and surrogate functions (with a gird of 30 times 30 combinations evaluated). Herein, four transports $\bar{\Lambda}, \overline{\Lambda'}, \bar{k}_0'$, and α_0 are plotted from (a) to (d), respectively. This illustrates again the above-stated convergence characteristics of the surrogates. In terms of computational cost, the evaluation of the cost function with the surrogate model took about 128 seconds for a grid of 100×100 sampling points. Proceeding with the reference multiscale solutions (where only one quarter of the PUC is used, by periodicity) requires about 39 hours with 30 sampling points along each direction.

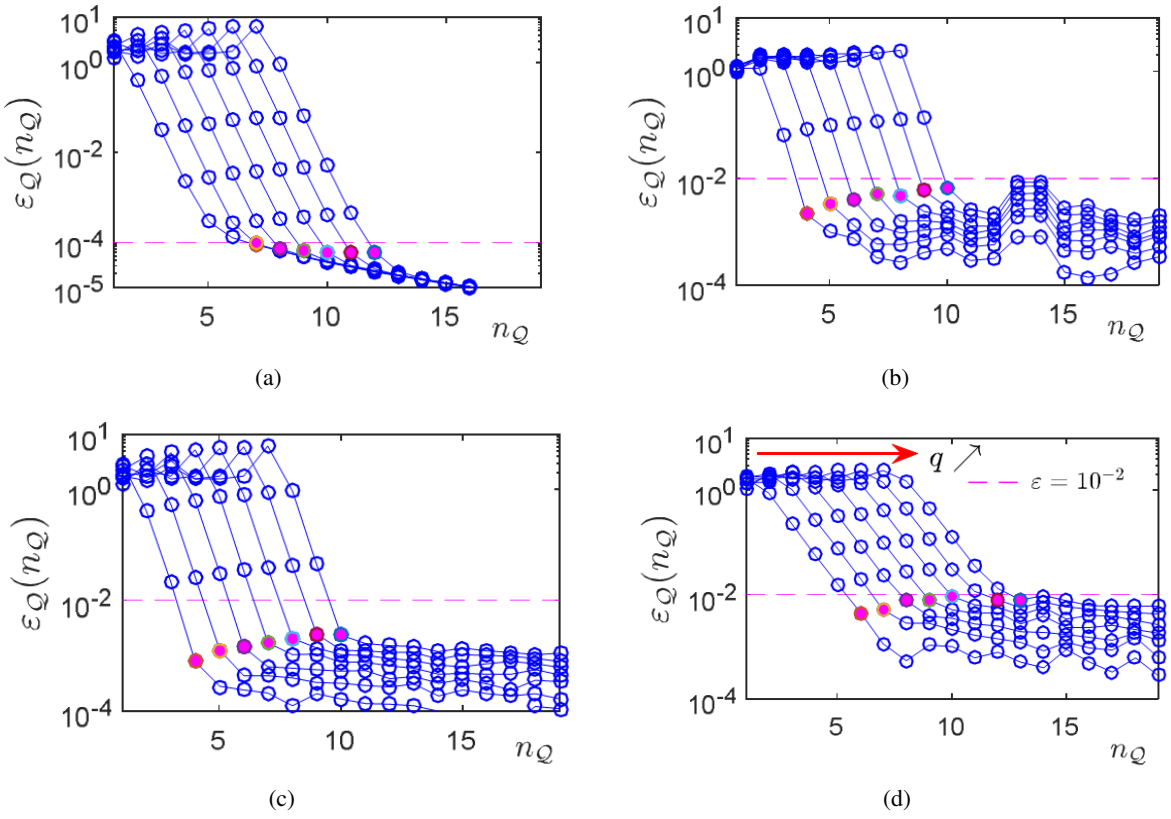

Figure 4. Graph of $n_Q \mapsto \varepsilon_{n_Q}(n_Q)$ for $p = 2k + 1$ with $2 \leq k \leq 8$. The results in sub-figures (a) to (d) are representative for factors $\overline{\Lambda'}, \overline{k_0}, \overline{k'_0}$, and α_α

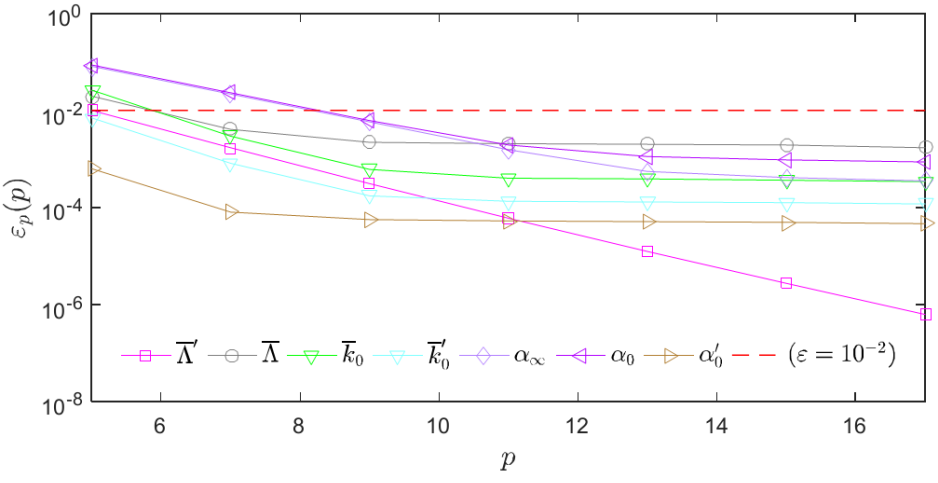

Figure 5. Graph of error map $p \mapsto \varepsilon_q(p)$ for $n_Q = 20$ and $p = 2k + 1$ with $2 \leq k \leq 8$

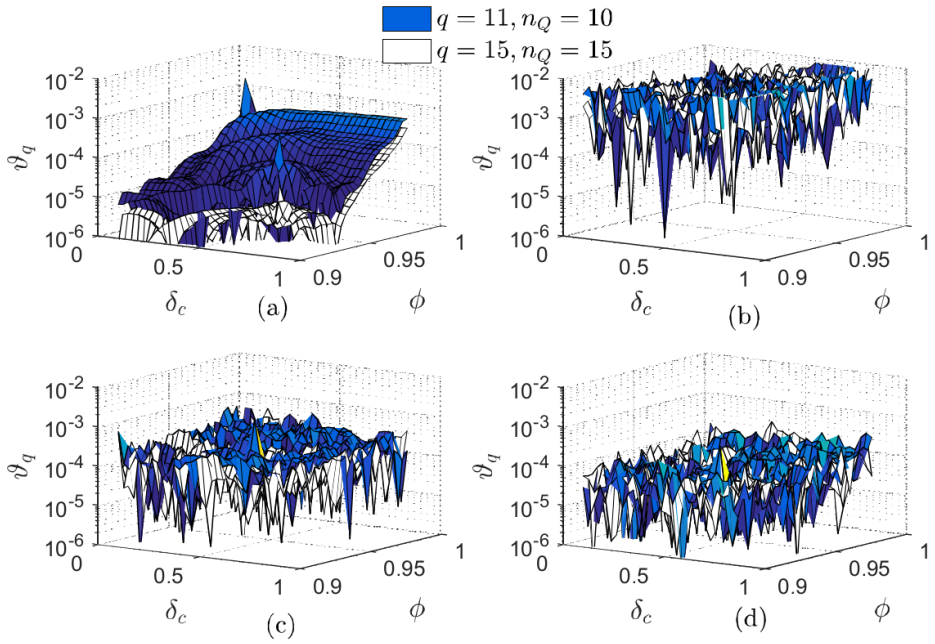

Figure 6. Graph of distance mapping $(\delta_c, \phi) \mapsto \vartheta_q(\delta_c, \phi)$ estimated with the polynomial expansions at order $p = 11$ (color surface) and $p = 15$ (while surface). The results are for $\bar{\Lambda}$, $\overline{\Lambda'}$, $\bar{k}'_0$, and α_0 from (a) to (d)

4.3. Acoustic properties of foam-based absorbers

Fig. 7 provides the effect of geometrical factors on foamy transport properties (cross makers: reference and lines: surrogates with $p = 11$ and $n_Q = 10$). The thicker lines are for porosities ranging from 0.9 to 0.99. Regardless of porosities under consideration, the factors of lengths and permeabilities decrease with an increase in the membrane ratio (Figs. 7(a)–(b)), while three tortuosity functions experience a sharp growth (Figs. 7(c)–(d)). These trends are in good agreement with the findings in Refs. [4, 6] and that can be explained by the reduction of the throat size in highly closed membrane foams. The lines track perfectly the markers that demonstrate good predictability of surrogates.

Next, the single-layer absorber is considered to illustrate the surrogate model in terms of predicting sound absorption. All predictions below are produced with foams with a cell size of 1 mm. Fig. 8 plots the sound absorption of foam layer within a thickness of 0.02 m with two porosities, $\phi = 0.90$ (left panel) and $\phi = 0.99$ (right panel). Arrow indicates an increase in δ_c from 0.1 to 0.9. The obtained curves reveal that the open porosity affects slightly the sound absorption behavior, while the membrane level has a significant effect. In addition, for foam nearly closed-cell structures its sound absorption behavior shows quarter-wavelength resonances at several frequencies, while the open-cell foam with low porosity provides a higher sound absorption compared with highly porosity foams.

In the next investigations, we only work with surrogate models of transport properties, and the sound absorptions are still estimated through the JCAPL model. The curves in Fig. 9 are for a case of foam with a porosity of 0.99, but the membrane level ranges from open cell to nearly close cell ones (i.e., [0.1 0.9]). Clearly, the thicker the absorber layer the better sound absorptions, and the membrane range providing a higher absorption is extended to a low value of nearly 0.92 (see the large zone with a high-value absorption in the right panel compared with the left one in Fig. 9).

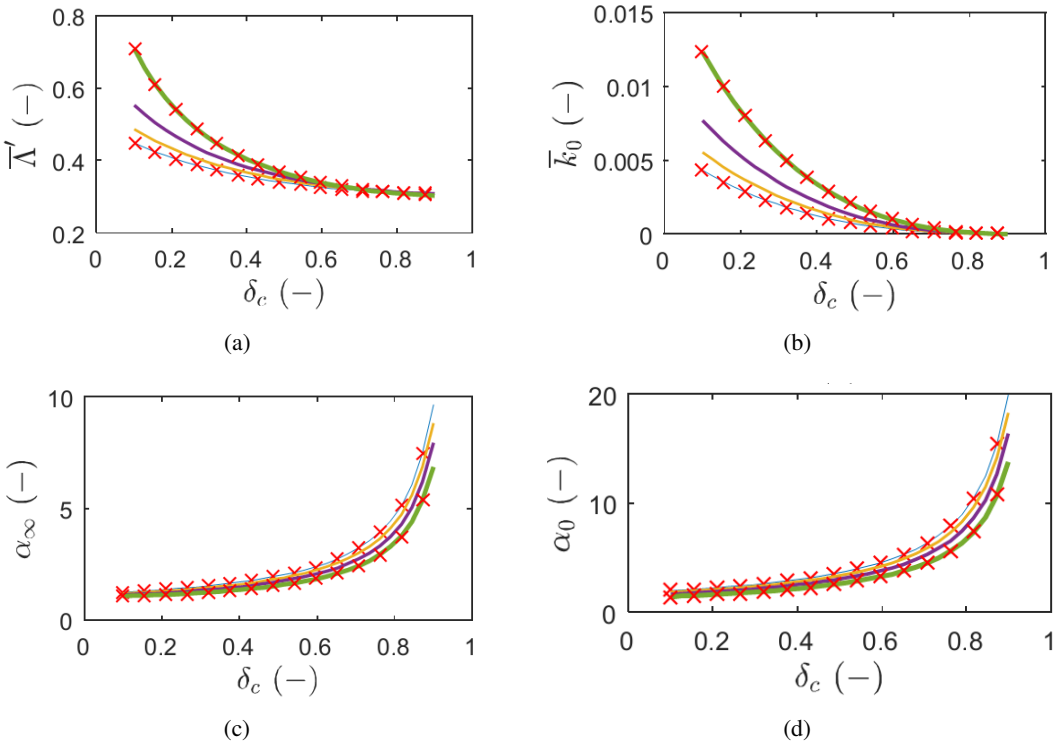

Figure 7. Effect of geometrical factors on transport properties: (cross markers) reference and (lines) surrogate values. The thicker the line the higher porosity

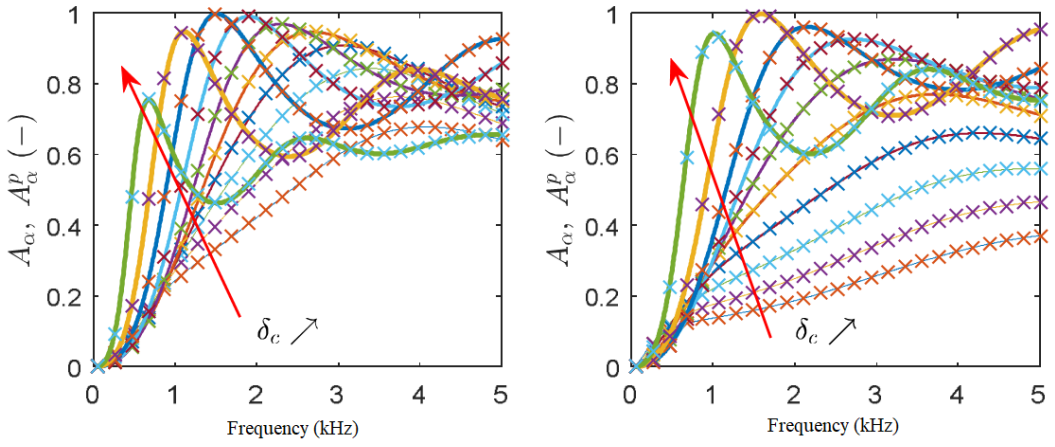

Figure 8. Effect of geometrical factors on the sound absorption properties for $\phi = 0.90$ (left) and $\phi = 0.99$ (right): (cross markers) reference and (lines) surrogate values

Finally, for designing sound absorbers, the averaging sound absorption index $\overline{A_\alpha} = 1/N \sum_{i=1}^{N} A_\alpha(\omega_i)$ is provided and defined from N discrete angular frequencies in the range of interest. Herein, we introduce three frequency bands, $[f_1, f_N]$ = [50 500], [500 1500], and [1500 4500] Hz, namely RF1 to

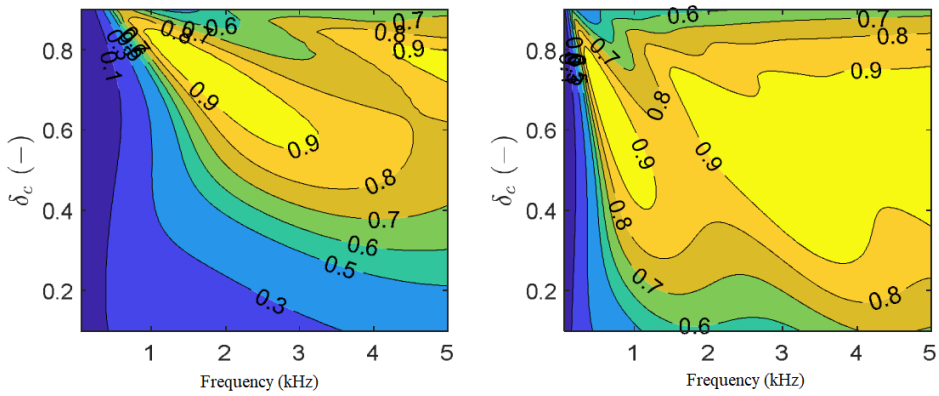

Figure 9. Sound absorption capacity of foam-based absorbers. Results correspond L = 20 mm (left part) and L = 60 mm (right part)

RF3. To continue with the foam having high porosity of 0.99 as shown in Fig. 8, but the moderated level of membrane (i.e., $\delta_c = 0.5$) is selected. It is seen from Fig. 10 that for a certain foam material, we can achieve successfully the sound absorption targets by varying only the layer thickness L. It is obvious that the challenging of low-frequency absorption is remarked for layers with $L < 80$ mm (i.e., $\overline{A_\alpha} < 0.4$), whereas a high-level absorption (i.e., $\overline{A_\alpha} > 0.8$) over both RF2 and RF3 ranges can be obtained via $L > 50$ mm.

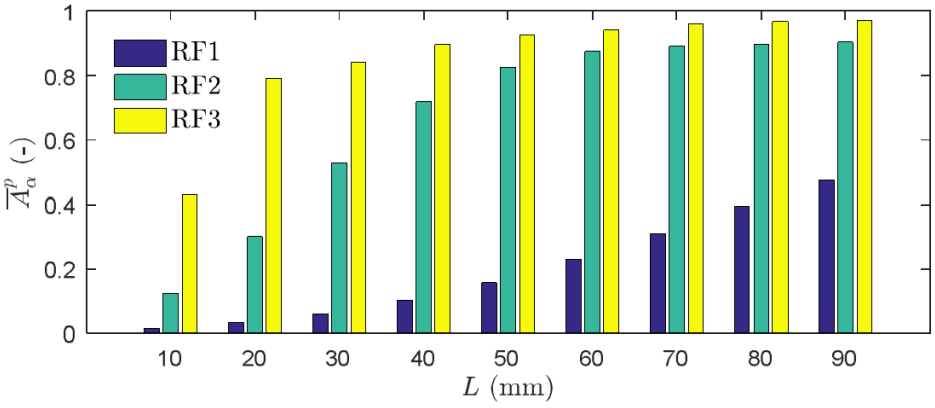

Figure 10. Sound absorption of absorbers with varying the layer thickness

5. Conclusions

The numerical and PCE-surrogate approach is proposed to characterize the microstructure-property correlations of acoustic cellular foams. The convergence characteristics of the surrogate models reveal that: (i) having a low computational cost, the surrogate can predict all transport properties within a tolerance error of 10^{-2}; (ii) using these surrogate maps of macroscopic transports, we can estimate accurately and efficiently the absorption property (at individual frequencies or over a whole range of interest) of foam structures over the design space. Finally, while the suggested application only dealt

with foam layers, it should be noticed that our framework can readily accommodate hybrid morphological structures (e.g., polydisperse/graded morphology, composite/multi-layered absorbers) where sparse grids should be employed instead of the regular full one.

Acknowledgments

This work is funded by the Vietnam National Foundation for Science and Technology Development (NAFOSTED) under grant number 107.01-2019.316.

References

[1] Cox, T., d'Antonio, P. (2016). *Acoustic absorbers and diffusers: theory, design and application*. CRC Press.

[2] Allard, J. F., Atalla, N. (2009). *Propagation of Sound in Porous Media*. John Wiley & Sons, Ltd.

[3] Vér, I. L., Beranek, L. L. (2005). *Noise and vibration control engineering: principles and applications*. John Wiley & Sons.

[4] Trinh, V. H., Langlois, V., Guilleminot, J., Perrot, C., Khidas, Y., Pitois, O. (2019). Tuning membrane content of sound absorbing cellular foams: Fabrication, experimental evidence and multiscale numerical simulations. *Materials & Design*, 162:345–361.

[5] Park, J., Yang, S. H., Minn, K. S., Yu, C. B., Pak, S. Y., Song, Y. S., Youn, J. R. (2018). Design and numerical analysis of syntactic hybrid foam for superior sound absorption. *Materials & Design*, 142: 212–220.

[6] Doutres, O., Atalla, N., Dong, K. (2013). A semi-phenomenological model to predict the acoustic behavior of fully and partially reticulated polyurethane foams. *Journal of Applied Physics*, 113(5):054901.

[7] Hilyard, N. C., Cunningham, A. (1994). *Low density cellular plastics*. Springer Netherlands.

[8] Boulvert, J., Cavalieri, T., Costa-Baptista, J., Schwan, L., Romero-García, V., Gabard, G., Fotsing, E. R., Ross, A., Mardjono, J., Groby, J.-P. (2019). Optimally graded porous material for broadband perfect absorption of sound. *Journal of Applied Physics*, 126(17):175101.

[9] Zieliński, T. G., Venegas, R., Perrot, C., Červenka, M., Chevillotte, F., Attenborough, K. (2020). Benchmarks for microstructure-based modelling of sound absorbing rigid-frame porous media. *Journal of Sound and Vibration*, 483:115441.

[10] Lee, C.-Y., Leamy, M. J., Nadler, J. H. (2009). Acoustic absorption calculation in irreducible porous media: A unified computational approach. *The Journal of the Acoustical Society of America*, 126(4): 1862.

[11] Gasser, S., Paun, F., Bréchet, Y. (2005). Absorptive properties of rigid porous media: Application to face centered cubic sphere packing. *The Journal of the Acoustical Society of America*, 117(4):2090–2099.

[12] Park, J. H., Yang, S. H., Lee, H. R., Yu, C. B., Pak, S. Y., Oh, C. S., Kang, Y. J., Youn, J. R. (2017). Optimization of low frequency sound absorption by cell size control and multiscale poroacoustics modeling. *Journal of Sound and Vibration*, 397:17–30.

[13] Gao, K., van Dommelen, J. A. W., Geers, M. G. D. (2016). Microstructure characterization and homogenization of acoustic polyurethane foams: Measurements and simulations. *International Journal of Solids and Structures*, 100-101:536–546.

[14] Doutres, O., Salissou, Y., Atalla, N., Panneton, R. (2010). Evaluation of the acoustic and non-acoustic properties of sound absorbing materials using a three-microphone impedance tube. *Applied Acoustics*, 71 (6):506–509.

[15] Olny, X., Panneton, R. (2008). Acoustical determination of the parameters governing thermal dissipation in porous media. *The Journal of the Acoustical Society of America*, 123(2):814–824.

[16] Panneton, R., Olny, X. (2006). Acoustical determination of the parameters governing viscous dissipation in porous media. *The Journal of the Acoustical Society of America*, 119(4):2027–2040.

[17] Nhu, N. T. H., Binh, T. A., Hung, H. M. (2020). A three-dimensional model for rain-wind induced vibration of stay cables in cable-stayed bridges. *Journal of Science and Technology in Civil Engineering (STCE) - NUCE*, 14(1):15–27.

[18] Trinh, V. H., Guilleminot, J., Perrot, C. (2018). On the Construction of Multiscale Surrogates for Design Optimization of Acoustical Materials. *Acta Acustica united with Acustica*, 104(1):1–4.

[19] Sohrabi, S. H., Ketabdari, M. J. (2020). Stochastic modeling and sensitivity analysis of underwater sound absorber rubber coating. *Applied Acoustics*, 164:107282.

[20] Trinh, V. H. (2018). Effect of membrane content on the acoustical properties of three-dimensional monodisperse foams: experimental, numerical and semi-analytical approaches. PhD thesis, Paris-Est University.

[21] Langlois, V., Trinh, V. H., Lusso, C., Perrot, C., Chateau, X., Khidas, Y., Pitois, O. (2018). Permeability of solid foam: Effect of pore connections. *Physical Review E*, 97(5):053111.

[22] Auriault, J.-L., Boutin, C., Geindreau, C., editors (2009). *Homogenization of Coupled Phenomena in Heterogenous Media*. ISTE.

[23] Boutin, C., Geindreau, C. (2008). Estimates and bounds of dynamic permeability of granular media. *The Journal of the Acoustical Society of America*, 124(6):3576–3593.

[24] Avellaneda, M., Torquato, S. (1991). Rigorous link between fluid permeability, electrical conductivity, and relaxation times for transport in porous media. *Physics of Fluids A: Fluid Dynamics*, 3(11):2529–2540.

[25] Johnson, D. L., Koplik, J., Dashen, R. (1987). Theory of dynamic permeability and tortuosity in fluid-saturated porous media. *Journal of Fluid Mechanics*, 176(-1):379.

[26] Rubinstein, J., Torquato, S. (1988). Diffusion-controlled reactions: Mathematical formulation, variational principles, and rigorous bounds. *The Journal of Chemical Physics*, 88(10):6372–6380.

[27] Lafarge, D., Lemarinier, P., Allard, J. F., Tarnow, V. (1997). Dynamic compressibility of air in porous structures at audible frequencies. *The Journal of the Acoustical Society of America*, 102(4):1995–2006.

[28] Champoux, Y., Stinson, M. R., Daigle, G. A. (1991). Air-based system for the measurement of porosity. *The Journal of the Acoustical Society of America*, 89(2):910–916.

[29] Sullivan, T. J. (2015). *Introduction to Uncertainty Quantification*. Springer International Publishing.

[30] Staber, B., Guilleminot, J. (2017). Functional approximation and projection of stored energy functions in computational homogenization of hyperelastic materials: A probabilistic perspective. *Computer Methods in Applied Mechanics and Engineering*, 313:1–27.

[31] Gasser, S. (2003). Etude des propriétés acoustiques et mécaniques d'un matériau métallique poreux modèle à base de sphères creuses de nickel. PhD thesis, Institut National Polytechnique de Grenoble-INPG.

[32] Venegas, R. (2011). Microstructure influence on acoustical properties of multiscale porous materials. PhD thesis, University of Salford, UK.